Jierong Wang, Y.-S. Su, M. Spitaler, K.M. Zoch, C. Krellner, P. Puphal, S. E. Brown, and A. Pustogow, **

Department of Physics and Astronomy, UCLA, Los Angeles, California 90095, USA
Institute of Solid State Physics, TU Wien, 1040 Vienna, Austria
Institute of Physics, Goethe-University Frankfurt, 60438 Frankfurt (Main), Germany
Amax-Planck-Institute for Solid State Research, 70569 Stuttgart, Germany

It is predicted that strongly interacting spins on a frustrated lattice may lead to a quantum disordered ground state or even form a quantum spin liquid with exotic low-energy excitations. However, a thorough tuning of the frustration strength, separating its effects from those of disorder and other factors, is pending. Here we break the symmetry of a kagome-lattice compound in a controlled manner by applying in situ uniaxial stress. The transition temperature of $Y_3Cu_9(OH)_{18}OCl_8$ is linearly enhanced with strain, $\Delta T_N/T_N \approx 10\%$ upon in-plane compression of order 1%, providing clear evidence for a release of frustration and its pivotal role for magnetic order. Our comprehensive ¹H NMR results suggest a $\overrightarrow{Q} = (1/3 \times 1/3)$ state under unstrained conditions and further reveal an incomplete antiferromagnetic transition with fluctuating moments in this strongly frustrated system.

Even after two decades of intense scrutiny, quantum spin liquids (QSL) remain an elusive state of matter [1– 4]. Apart from growing evidence for the importance of disorder [5–15], geometrical frustration is considered decisive to suppress magnetic order in presence of strong antiferromagnetic (AFM) exchange interactions. vast majority of QSL candidates are found in quasi twodimensional correlated electron systems with triangular [8, 16-21], honeycomb [22] or kagome [23, 24] lattices. Herbertsmithite, ZnCu₃(OH)₆Cl₂, is an archetype realization of the latter symmetry [24] and has been intensely studied over the last two decades [5, 24-31] - not least due to the exciting proposal of exotic superconductivity and Dirac bands in a doped kagome lattice [32]. Although the latter scenario could not be realized so far [33], many related compounds substituting Zn by other bi- or trivalent cations have been synthesized by now [23]. Among those, Y₃Cu₉(OH)₁₈OCl₈ [34] (denoted as Y-kapellasite) and YCu₃(OH)₆Cl₃ [35] crystallize in the closely-related kapellasite structure (see Fig. 1) and exhibit AFM order at temperatures $T_{\rm N} \ll J/k_{\rm B} \approx 10^2 {\rm K}.$

So far, most attempts to modify the frustration strength focused on chemical substitution in order to arrange the valence electrons in the above mentioned patterns. While commonly physical pressure is applied to tune electronic interactions, e.g. towards metal-insulator transitions, hydrostatic compression does not directly affect the lattice symmetry, unless it triggers a structural transition. Recent developments in piezoelectric uniaxial strain applications at cryogenic temperatures [36, 37] now provide us the opportunity to modify the degree of geometrical frustration in a controlled manner.

Here, we take full advantage of uniaxial strain to directly tune magnetic order in Y-kapellasite single crystals. We characterize the magnetic properties by $^1\mathrm{H}$ nuclear magnetic resonance (NMR) in a temperature range 1.5–200 K and reveal strong spin correlations for T < 30 K. We find AFM below $T_{\mathrm{N}} = 2.2$ K that is consistent with the proposed $\overrightarrow{Q} = (1/3 \times 1/3)$ order [38]. By

applying uniaxial strain of order 1% we tune the exchange interactions and frustration strength in situ triggering a pronounced increase of $T_{\rm N}$ linear with strain.

In the two Y analogs of herbertsmithite (kapellasite), the additional charge upon substitution of Zn²⁺ is compensated, resulting in Mott insulators with a chargetransfer gap of 3 eV ($U \approx 8$ eV [39]). In the case of YCu₃(OH)₆Cl₃ this leads to an unstable crystal structure - similar to GaCu₃(OH)₆Cl₃ [33] it can be only synthesized as powder [35, 40] – while large Y₃Cu₉(OH)₁₈OCl₈ single crystals with slightly distorted kagome layers (structure shown in Fig. 1) can be grown by hydrothermal methods [34]. Both compounds exhibit AFM order at temperatures much lower than $\Theta_{CW} \approx 100$ K; magnetization, specific heat, μ -SR and neutron diffraction experiments yield $T_N = 2.2 \text{ K}$ for Y-kapellasite [34, 40], related with the observation of THz magnons [41], and $T_{\rm N} = 15 \text{ K for YCu}_3({\rm OH})_6{\rm Cl}_3 [35, 40, 42, 43].$ Despite the apparent absence of a QSL state down to $T \to 0$, distorted kagome lattices [44–47] came into focus recently due to magnetoelastic coupling and the realization of

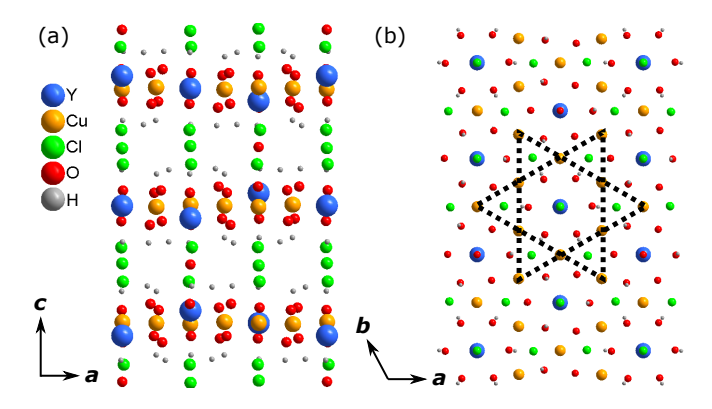


FIG. 1. Crystal structure of $Y_3Cu_9(OH)_{18}OCl_8$ (Y-kapellasite). (a) Cu^{2+} atoms (orange) are arranged in layers parallel to the ab-plane. (b) Within the plane they form a S=1/2 kagome lattice indicated by black dotted lines.

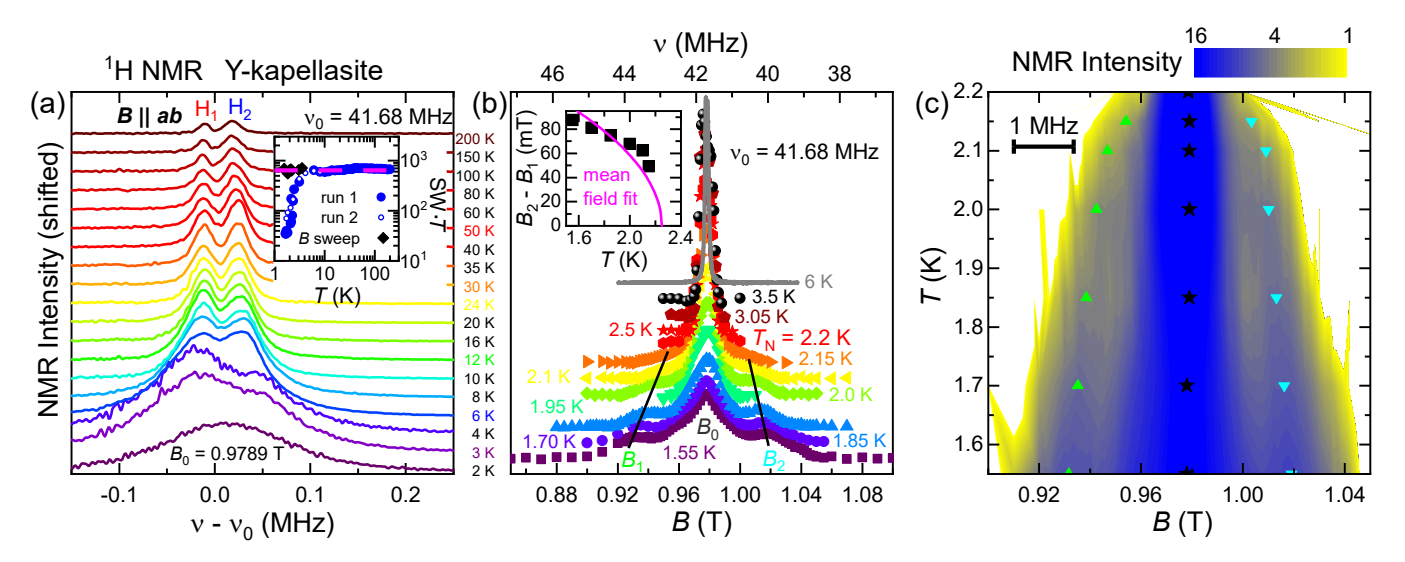


FIG. 2. (a) The ¹H NMR spectra acquired for in-plane magnetic field ($B \perp a$, $B_0 = 0.9789$ T) consist of two peaks (H_1 , H_2) separated by 30–40 kHz. The lines exhibit successive broadening upon cooling and exceed the experimental bandwidth below 4 K, as seen by the deviation of the integrated spectral weight SW from the standard T^{-1} dependence (inset). (b) The spectra below 4 K, acquired by magnetic field sweeps at constant frequency $\nu_0 = 41.68$ MHz, reveal a pronounced splitting into three peaks below $T_N = 2.2$ K. The separation between the two outer peaks (B_1 , B_2) increases to lower temperatures (inset) while the central peak remains at B_0 . The grey line indicates the spectrum at 6 K, which follows the frequency scale at the top. (c) The false-color plot of the data from panel (b) illustrates the shifting of B_1 and B_2 as well as the strong broadening. The horizontal bar corresponds to a frequency of $\Delta \nu = \Delta B/^1 \gamma = 1$ MHz.

non-trivial ground states such as pinwheel [48, 49] and $\overrightarrow{Q} = (1/3 \times 1/3)$ order [38].

Prior to application of strain we carried out a thorough ambient-pressure NMR characterization of Y-kapellasite. The magnetic field was aligned parallel to the Cu²⁺ chains of the kagome network, i.e. perpendicular to the crystallographic a-axis; in the following, this inplane field configuration is denoted as $B \parallel ab$. Fig. 2a presents the temperature evolution of the ¹H spectra $(B_0 = 0.9789 \text{ T}, \nu_0 = 41.68 \text{ MHz})$, yielding two peaks separated by 30-40 kHz above 4 K. At lower temperatures, the line broadening exceeds the experimental bandwidth such that the intensity (probed by integrating the spectral weight SW; shown in inset of Fig. 2a) deviates from the standard T^{-1} dependence. To resolve the entire peak structure, we performed magnetic field sweeps at constant frequency ν_0 covering the temperature range between 1.55 K and 3.5 K (Fig. 2b,c). Below $T_{\rm N}$ the signal splits into a triplet: while the central line (B_0) remains unshifted, the two outer peaks (B_1, B_2) move apart symmetrically upon cooling. As plotted in the inset, the separation B_2-B_1 is consistent with the onset of a broken symmetry, which is further illustrated by the yellow-blue contour plot in Fig. 2c. On a quantitative level, the line splitting at the lowest measured temperature agrees well with a local field $B_{loc} \approx 60 - 64 \text{ mT}$ originating from dipolar coupling between ¹H nuclear moments and AFM ordered electron spins on the Cu²⁺ sites (see Fig. 1), which are at a distance 2.44–2.50 Å [34].

While our observation of a line splitting evidences

AFM order setting in at T_N , the ratio among the peak intensities provides insight into the details of the spin structure. Upon $\overline{Q} = (1/3 \times 1/3)$ order predicted for a distorted kagome lattice [38], along a Cu²⁺ chain four successive AFM bonds are satisfied followed by two unsatisfied bonds. We point out that ¹H nuclei are ideal probes of the local field at a bond as they are attached to oxygen atoms and, hence, are sitting between two neighboring Cu²⁺ sites, as sketched in Fig. 3a. If the electron spins are antiparallel, their local fields cancel out yielding a proton resonance at B_0 ; for parallel alignment, their local fields add up to (subtract from) the external field yielding the NMR line at B_1 (B_2). Our Gaussian fits in Fig. 3b indeed reveal an intensity ratio between $B_0:B_1:B_2$ sites of 4:0.93:1.07 that is close to 4:1:1 [50]. Overall, the spectral features of our NMR measurements are consistent with $\overrightarrow{Q} = (1/3 \times 1/3)$ order in Y-kapellasite [38] and motivate more thorough assessment of this model.

Apart from the splitting, the NMR linewidth (Fig. 3c) is subject to severe broadening. The full width at half maximum (FWHM) increases beyond the homogeneous linewidth $(\pi T_2)^{-1}\approx 35$ kHz already for T<30 K, indicating the onset of antiferromagnetic fluctuations, followed by an abrupt broadening at $T_{\rm N}$. Note, while the FWHM increases by two orders of magnitude across the studied temperature range, the spin-spin relaxation rate merely varies by a factor two. The two-peak structure of the spectrum (T>4 K) and the absolute values of T_2 are caused by proton-proton dipolar coupling since hyperfine coupling to the spin-1/2 ${\rm Cu}^{2+}$ sites is weak.

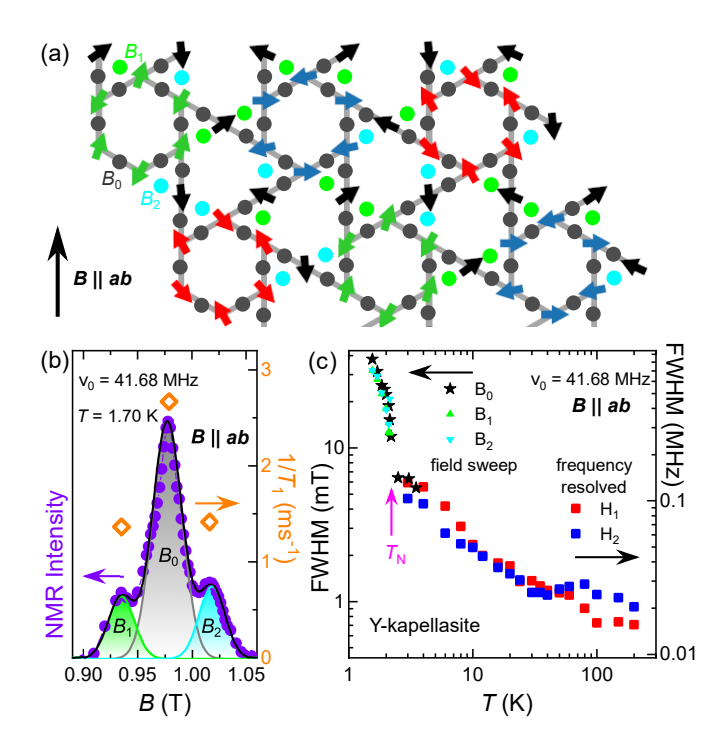


FIG. 3. (a) $Q=(1/3\times 1/3)$ AFM order predicted for a distorted kagome lattice [38]. Colored circles indicate location of $^1\mathrm{H}$ nuclei in the crystal lattice of Y-kapellasite (cf. Fig. 1). (b) The NMR intensity (violet) at 1.7 K was fitted with three Gaussian peaks corresponding to the $^1\mathrm{H}$ positions (see color) in (a); their intensity scales as 4:0.93:1.07 ($B_0:B_1:B_2$). The spin-lattice relaxation rate (orange diamonds) was measured at different fields: T_1^{-1} of the side peaks (B_1 , B_2) is $\approx 50\%$ smaller than for the central peak at $B_0=0.9789$ T. (c) The full width at half maximum (FWHM), extracted for the $^1\mathrm{H}$ NMR peaks H_1 and H_2 ($T>T_N$; see Fig. 2a) as well as for the three lines B_0 , B_1 and B_2 emerging below T_N (see Fig. 2b,c), exceeds the homogeneous linewidth below 30 K and shows a steep increase at T_N . Note the different units of the vertical scales.

Hence, we assign the pronounced line broadening below 30 K to magnetic correlations in Y-kapellasite.

Aside from T_2 effects, the spin-lattice relaxation rate T_1^{-1} is highly susceptible to the emerging magnetism. Above 10 K the ¹H relaxation rate of Y-kapellasite, plotted in Fig. 4, is of similar magnitude compared to $\operatorname{ZnCu_3}(\operatorname{OH})_6\operatorname{Cl_2}$ [51]. However, herbertsmithite exhibits a different temperature dependence with a maximum around 90 K and steadily decreasing T_1^{-1} upon cooling below that (magenta dotted line in Fig. 4). Here, we observe a positive slope at high temperatures, likely related to lattice dynamics, while below 30 K the relaxation rate increases upon cooling due to AFM fluctuations. Down to 4 K we do not observe pronounced field dependence or anisotropy (measurements for $B \parallel c$ shown in inset of Fig. 4) in T_1^{-1} .

The onset of magnetic order yields a sharp peak at the transition temperature $T_{\rm N}=2.2$ K. Increasing the

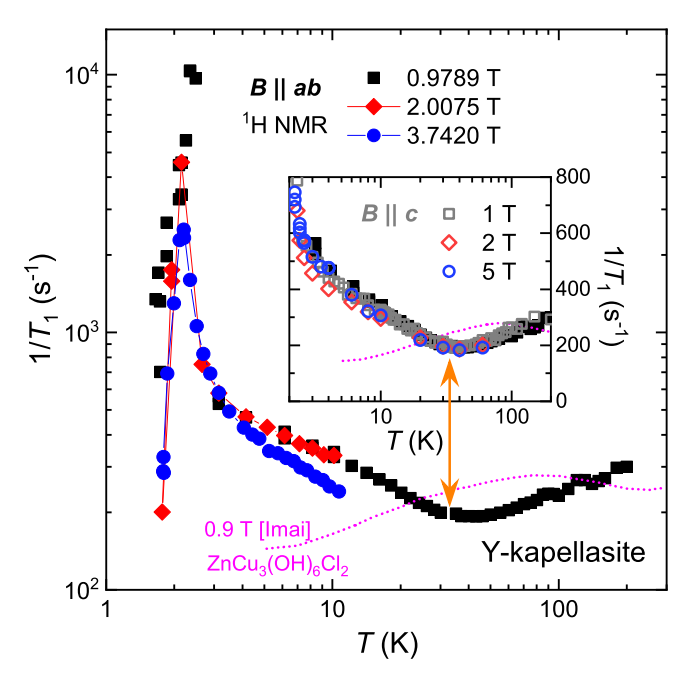


FIG. 4. ¹H NMR spin-lattice relaxation rate T_1^{-1} for $B \parallel ab$ and $B \parallel c$ (inset). Upon cooling from room temperature, T_1^{-1} initially decreases towards a minimum around 32 K (orange double arrow). Below that, the increase of T_1^{-1} signals the onset of strong antiferromagnetic spin fluctuations, which result in a sharp maximum at $T_N = 2.2$ K. Increasing the magnetic field yields a reduced peak value and broadening of the transition, consistent with specific heat results [34]. Above 4 K T_1^{-1} does not exhibit pronounced field dependence or anisotropy.

magnetic field to 2 T and 3.7 T decreases the peak values of T_1^{-1} and broadens the maximum, in accord with specific heat results [34]. As AFM sets in, relaxation rapidly decreases upon further cooling. Throughout, we determined the temperature dependence of T_1^{-1} at B_0 . At 1.70 K we also measured T_1^{-1} at the two outer peaks B_1 and B_2 (Fig. 3b) yielding a 50% smaller value compared to B_0 . The faster relaxation at the central peak indicates fluctuating spins – possibly a small portion that has evaded (or is not involved in) static AFM order. In this regard, NMR measurements at lower temperatures are highly desired, especially at $T \ll 1$ K.

To summarize the findings so far, the NMR properties are consistent with AFM order of $\overrightarrow{Q}=(1/3\times 1/3)$ symmetry [38]. Moreover, Y-kapellasite features coexistence of fluctuating and static moments, in line with recent μ -SR results [40]. The spin-lattice relaxation rate is highly susceptible to the onset of magnetic order and exhibits a sharp peak at the transition, making it a sensitive probe of the transition temperature. Having identified its unusual magnetic ground state, in the following we apply in-plane uniaxial stress to Y-kapellasite single crystals. Through distorting the kagome lattice by compression along the Cu²⁺ chains, as sketched in Fig. 5d, we directly modify the anisotropy of the transfer integrals t'/t and,

hence, the exchange interactions J, J' and their degree of geometrical frustration.

In Fig. 5 we trace the change in transition temperature through T_1^{-1} measurements at $B_0 = 1.81 \text{ T } (B \parallel a)$ upon applying uniaxial stress parallel to the Cu²⁺ chains. There is a clear enhancement of T_N with approximately linear dependence on the applied strain, which agrees with calculations of Heisenberg AFM ordering on a distorted kagome lattice [52]. Our results on two samples consistently reveal an increase of transition temperature by almost 10% for compressive strain of order 1% parallel to the kagome layers. How does this compare with the modifications expected for hydrostatic pressure of similar size? For comparison, we consider that the superexchange is proportional to $t^4/(\Delta^2 U)$ and $t \propto r^{-4}$, hence 1% reduction of Cu-Cu distance should result in an increase of 16%. However, this is a large overestimate, because in real materials the crystal lattice adapts mostly by changing bond angles rather than bond length [53]. Thus, we conclude that the major effect arises from releasing frustration of the kagome lattice.

Let us assess the observed strain-tuning effects in the context of other materials where the structure impacts the magnetic properties. In ZnCu₃(OH)₆Cl₂, indications of DM interaction [24, 29] and even symmetry breaking [54, 55] have been reported, likely related to magnetoelastic coupling [56]. Hydrostatic pressure yields an emergence of magnetic order [57], but also a field-induced spin freezing was reported [58]. The compound studied here shows structural similarities to the 'pin-wheel' kagome structure of Rb₂Cu₃SnF₁₂ [48, 59] and a Barlowite polymorph [49]. To that end, Y-kapellasite is likely frustrated in a different way than Herbertsmithite or Kapellasite, which both exhibit an undistorted kagome lattice – at the expense of severe Zn/Cu antisite disorder [6]. Finally, an indication for a structural involvement in the magnetic degrees of freedom is the onset of spin fluctuations below a recently discovered structural anomaly at 32 K [60]. An intriguing scenario could be that this is the onset of nematic order below a crossover at $T^* \gg T_N$ predicted for a distorted kagome lattice [52]. Extending our present strain-tuning experiments on Y-kapellasite to higher temperatures would enable direct scrutiny of this issue and thus remains a desideratum for future work.

To conclude, we performed comprehensive $^1\mathrm{H}$ NMR investigations on Y-kapellasite as a function of temperature, magnetic field and uniaxial stress. Under unstrained conditions we find spectral evidence for AFM order of $\overrightarrow{Q} = (1/3 \times 1/3)$ type below $T_\mathrm{N} = 2.2~\mathrm{K}$ in this distorted kagome compound. Clear signatures for AFM are also seen in the linewidth and spin-lattice relaxation rate, which are dominated by proton dynamics at elevated temperatures while magnetic correlations become dominant below 30 K. Based on this characterization, we applied in situ uniaxial stress parallel to the kagome layers, resulting in a linear increase of T_N with strain,

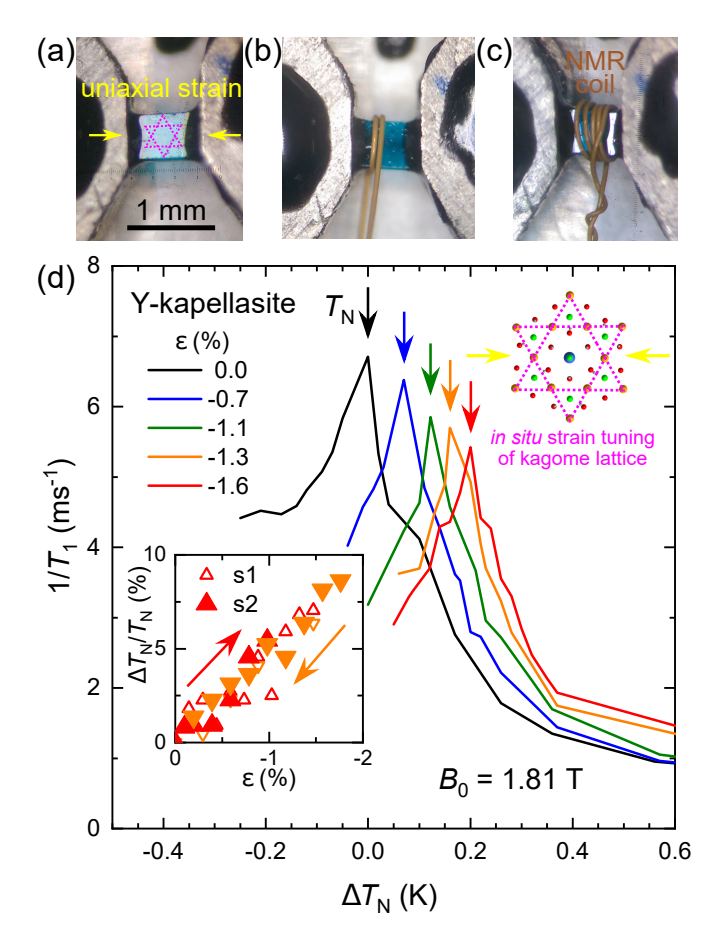


FIG. 5. (a-c) For NMR experiments under uniaxial strain a single crystal was glued between the two arms of a piezoelectric strain cell (a) and, subsequently, an NMR coil was wound around it (b,c). (d) T_1^{-1} was measured for $B \parallel a$ upon uniaxial compression of the kagome lattice parallel to the Cu²⁺ chains (sketched on top right; cf. Fig. 1). Inset: in-plane strain of 1.5% results in a considerable enhancement of the transition temperature by $\Delta T_{\rm N}/T_{\rm N} \approx 10\%$.

in accord with theoretical predictions [52]. Through a controlled release of frustration, our findings evidence its crucial importance for correlated quantum magnets and spin liquids, opening the door for similar studies in triangular, honeycomb and other kagome materials. The pioneering strain-tuning approach presented here is ideally suited to resolve the magnetic ground states of existing materials, and to discover novel exotic spin phases beyond state-of-the-art theoretical frameworks [2, 4].

METHODS

NMR experiments were performed using variable temperature 4 He cryostats and superconducting magnets. At $T \geq 4$ K magnetic field and frequency were fixed according to the 1 H resonance condition $\nu_0 = ^1 \gamma B$, with $^1\gamma = 42.5774$ MHz/T, as the proton NMR spec-

trum was resolved within the experimental bandwidth. Due to excessive line broadening below 4 K, the NMR intensity started to drop below the expected T^{-1} behavior, as illustrated by blue circles in the inset of Fig. 2a that correspond to the integrated spectral weight (SW)of the NMR spectrum. To that end, at T < 4 K the ¹H spectra were acquired by sweeping the external field in dense intervals around $B_0=0.9789~\mathrm{T.}$ As illustrated by the black diamonds in the inset of Fig. 2a, the entire NMR intensity was recovered in these field-sweep measurements: in the inspected field range the total SW of the ${}^{1}\mathrm{H}$ resonance lines up with the T^{-1} behavior extrapolated from $T \geq 4$ K. Zero-strain NMR measurements were performed using large single crystals $(3 \times 2 \times 1 \text{ mm}^3)$. The relaxation measurements (Fig. 4) for in-plane (measured at UCLA) and out-of plane (acquired at TU Wien on a different sample) crystal axes show similar T_1^{-1} values. The relaxation rate T_1^{-1} was acquired at the central line (ν_0 , B_0 in Fig. 2b). At T=1.70 K we measured T_1^{-1} at $\nu_0 = 41.68$ MHz also for the two satellite peaks B_1 and B_2 obtaining values approximately 50% of T_1^{-1} at $B_0 = 0.9789$ T (orange symbols in Fig. 3b).

Uniaxial strain experiments were performed using piezoelectric strain cells (Razorbill) in the same ⁴He cryostat as the zero-strain studies for in-plane magnetic fields. For that, the Y-kapellasite sample (the single crystal shown in Fig. 5a-c was cut in dimensions $2.5 \times 0.45 \times 0.24 \text{ mm}^3$ with the longest dimension parallel to the Cu chains of the kagome layer, i.e. $\varepsilon \perp a$) was glued at room temperature on the strain cell using Stvcast and dried for several days. Here, the magnetic field direction was parallel to the a-axis, i.e. perpendicular to the in-plane fields in Fig. 2. Still, we observed a similar peak in T_1^{-1} at T_N for both $B \parallel a$ (Fig. 5) and $B \parallel ab$ (Fig. 4), hence our measurements of the relaxation rate were suitable to trace the strain dependence of the AFM transition. The strain voltage was varied at 4 K and successively T_1^{-1} was measured upon cooling through the transition, both for increasing and decreasing strain as indicated by red and orange symbols in Fig. 5d, respectively. The compression was monitored in situ by the built-in capacitive displacement sensor. Similar to previous strain studies [61, 62], the applied strain ε was calculated as the displacement divided by the length of the sample surface that remained free of epoxy – for sample s2 this corresponds to 0.6 mm (Fig. 5a-c). The linear increase of $T_{\rm N}$ with strain shown in the inset of Fig. 5d lines up for the two samples. Still, we do not exclude that the real compression of the sample is somewhat lower than the present estimate using the built-in capacitive sensor, likely $\varepsilon_{real} \approx 1\%$; also in Sr_2RuO_4 the strain of the van Hove singularity was first estimated as 0.6% [61, 63] and later corrected to 0.44% by using high-precision stressstrain sensors [64].

We thank M. R. Norman, M. Dressel, H. Jeschke and I. I. Mazin for useful comments and discussions. Sup-

port with sample preparation by G. Untereiner is kindly appreciated. A. P. acknowledges support by the Alexander von Humboldt Foundation through the Feodor Lynen Fellowship. Work at UCLA was supported by the National Science Foundation (DMR-2004553).

- * pustogow@ifp.tuwien.ac.at
- [1] L. Balents, Spin liquids in frustrated magnets., Nature **464**, 199 (2010).
- [2] L. Savary and L. Balents, Quantum spin liquids: a review, Rep. Prog. Phys. 80, 016502 (2017).
- [3] Y. Zhou, K. Kanoda, and T.-K. Ng, Quantum spin liquid states, Rev. Mod. Phys. 89, 25003 (2017).
- [4] C. Broholm, R. J. Cava, S. A. Kivelson, D. G. Nocera, M. R. Norman, and T. Senthil, Quantum spin liquids, Science 367, eaay0668 (2020).
- [5] A. Olariu, P. Mendels, F. Bert, F. Duc, J. C. Trombe, M. A. de Vries, and A. Harrison, ¹⁷O NMR Study of the Intrinsic Magnetic Susceptibility and Spin Dynamics of the Quantum Kagome Antiferromagnet ZnCu₃(OH)₆Cl₂, Phys. Rev. Lett. **100**, 87202 (2008).
- [6] D. E. Freedman, T. H. Han, A. Prodi, P. Müller, Q.-Z. Huang, Y.-S. Chen, S. M. Webb, Y. S. Lee, T. M. Mc-Queen, and D. G. Nocera, Site Specific X-ray Anomalous Dispersion of the Geometrically Frustrated Kagomé Magnet, Herbertsmithite, ZnCu3(OH)6Cl2, J. Am. Chem. Soc. 132, 16185 (2010).
- [7] Z. Zhu, P. A. Maksimov, S. R. White, and A. L. Chernyshev, Disorder-Induced Mimicry of a Spin Liquid in YbMgGaO₄, Phys. Rev. Lett. 119, 157201 (2017).
- [8] Y. Li, D. Adroja, R. I. Bewley, D. Voneshen, A. A. Tsirlin, P. Gegenwart, and Q. Zhang, Crystalline Electric-Field Randomness in the Triangular Lattice Spin-Liquid YbMgGaO₄, Phys. Rev. Lett. 118, 107202 (2017).
- [9] I. Kimchi, A. Nahum, and T. Senthil, Valence Bonds in Random Quantum Magnets: Theory and Application to YbMgGaO₄, Phys. Rev. X 8, 31028 (2018).
- [10] T. Itou, E. Watanabe, S. Maegawa, A. Tajima, N. Tajima, K. Kubo, R. Kato, and K. Kanoda, Slow dynamics of electrons at a metal-Mott insulator boundary in an organic system with disorder, Sci. Adv. 3, e1601594 (2017).
- [11] K. Riedl, R. Valentí, and S. M. Winter, Critical spin liquid versus valence-bond glass in a triangular-lattice organic antiferromagnet, Nat. Commun. 10, 2561 (2019).
- [12] A. Pustogow, T. Le, H.-H. Wang, Y. Luo, E. Gati, H. Schubert, M. Lang, and S. E. Brown, Impurity moments conceal low-energy relaxation of quantum spin liquids, Phys. Rev. B 101, 140401(R) (2020).
- [13] R. W. Smaha, I. Boukahil, C. J. Titus, J. M. Jiang, J. P. Sheckelton, W. He, J. Wen, J. Vinson, S. G. Wang, Y.-S. Chen, S. J. Teat, T. P. Devereaux, C. Das Pemmaraju, and Y. S. Lee, Site-specific structure at multiple length scales in kagome quantum spin liquid candidates, Phys. Rev. Mater. 4, 124406 (2020).
- [14] B. Miksch, A. Pustogow, M. Javaheri Rahim, A. A. Bardin, K. Kanoda, J. A. Schlueter, R. Hübner, M. Scheffler, and M. Dressel, Gapped magnetic ground state in quantum spin liquid candidate κ-(BEDT-TTF)₂Cu₂(CN)₃, Science 372, 276 LP (2021).

- [15] A. Pustogow, Thirty-Year Anniversary of κ -(BEDT-TTF)₂Cu₂(CN)₃: Reconciling the Spin Gap in a Spin-Liquid Candidate (2022).
- [16] Y. Shimizu, K. Miyagawa, K. Kanoda, M. Maesato, and G. Saito, Spin Liquid State in an Organic Mott Insulator with a Triangular Lattice, Phys. Rev. Lett. 91, 107001 (2003).
- [17] T. Isono, H. Kamo, A. Ueda, K. Takahashi, M. Kimata, H. Tajima, S. Tsuchiya, T. Terashima, S. Uji, and H. Mori, Gapless Quantum Spin Liquid in an Organic Spin-1/2 Triangular-Lattice κ-H₃(Cat-EDT-TTF)₂, Phys. Rev. Lett. 112, 177201 (2014).
- [18] Y. Shimizu, T. Hiramatsu, M. Maesato, A. Otsuka, H. Yamochi, A. Ono, M. Itoh, M. Yoshida, M. Takigawa, Y. Yoshida, and G. Saito, Pressure-Tuned Exchange Coupling of a Quantum Spin Liquid in the Molecular Triangular Lattice κ-(ET)₂Ag₂(CN)₃, Phys. Rev. Lett. 117, 107203 (2016).
- [19] T. Itou, A. Oyamada, S. Maegawa, and R. Kato, Instability of a quantum spin liquid in an organic triangular-lattice antiferromagnet, Nat. Phys. 6, 673 (2010).
- [20] Y. Shen, Y.-D. Li, H. Wo, Y. Li, S. Shen, B. Pan, Q. Wang, H. C. Walker, P. Steffens, M. Boehm, Y. Hao, D. L. Quintero-Castro, L. W. Harriger, M. D. Frontzek, L. Hao, S. Meng, Q. Zhang, G. Chen, and J. Zhao, Evidence for a spinon Fermi surface in a triangular-lattice quantum-spin-liquid candidate, Nature 540, 559 (2016).
- [21] Y. Xu, J. Zhang, Y. S. Li, Y. J. Yu, X. C. Hong, Q. M. Zhang, and S. Y. Li, Absence of Magnetic Thermal Conductivity in the Quantum Spin-Liquid Candidate YbMgGaO₄, Phys. Rev. Lett. 117, 267202 (2016).
- [22] H. Takagi, T. Takayama, G. Jackeli, G. Khaliullin, and S. E. Nagler, Concept and realization of Kitaev quantum spin liquids, Nat. Rev. Phys. 1, 264 (2019).
- [23] P. Puphal, K. M. Zoch, J. Désor, M. Bolte, and C. Krellner, Kagome quantum spin systems in the atacamite family, Phys. Rev. Mater. 2, 63402 (2018).
- [24] M. R. Norman, Colloquium: Herbertsmithite and the search for the quantum spin liquid, Rev. Mod. Phys. 88, 041002 (2016).
- [25] R. S. W. Braithwaite, K. Mereiter, W. H. Paar, and A. M. Clark, Herbertsmithite, Cu3Zn(OH)6Cl2, a new species, and the definition of paratacamite, Mineral. Mag. 68 (2004).
- [26] M. P. Shores, E. A. Nytko, B. M. Bartlett, and D. G. Nocera, A structurally perfect S = (1/2) kagomé antiferromagnet., J. Am. Chem. Soc. 127, 13462 (2005).
- [27] T.-H. Han, J. S. Helton, S. Chu, D. G. Nocera, J. A. Rodriguez-Rivera, C. Broholm, and Y. S. Lee, Fractionalized excitations in the spin-liquid state of a kagomelattice antiferromagnet, Nature 492, 406 (2012).
- [28] M. Fu, T. Imai, T.-H. Han, and Y. S. Lee, Evidence for a gapped spin-liquid ground state in a kagome Heisenberg antiferromagnet, Science 350, 655 LP (2015).
- [29] A. Zorko, M. Herak, M. Gomilšek, J. van Tol, M. Velázquez, P. Khuntia, F. Bert, and P. Mendels, Symmetry Reduction in the Quantum Kagome Antiferromagnet Herbertsmithite, Phys. Rev. Lett. 118, 17202 (2017).
- [30] P. Khuntia, M. Velazquez, Q. Barthélemy, F. Bert, E. Kermarrec, A. Legros, B. Bernu, L. Messio, A. Zorko, and P. Mendels, Gapless ground state in the archetypal quantum kagome antiferromagnet ZnCu3(OH)6Cl2, Nat. Phys. 16, 469 (2020).
- [31] J. Wang, W. Yuan, P. M. Singer, R. W. Smaha, W. He,

- J. Wen, Y. S. Lee, and T. Imai, Emergence of spin singlets with inhomogeneous gaps in the kagome lattice Heisenberg antiferromagnets Zn-barlowite and herbertsmithite, Nat. Phys. 10.1038/s41567-021-01310-3 (2021).
- [32] I. I. Mazin, H. O. Jeschke, F. Lechermann, H. Lee, M. Fink, R. Thomale, and R. Valentí, Theoretical prediction of a strongly correlated Dirac metal, Nat. Commun. 5, 10.1038/ncomms5261 (2014).
- [33] P. Puphal, K. M. Ranjith, A. Pustogow, M. Müller, A. Rogalev, K. Kummer, J.-C. Orain, C. Baines, M. Baenitz, M. Dressel, E. Kermarrec, F. Bert, P. Mendels, and C. Krellner, Tuning of a Kagome Magnet: Insulating Ground State in Ga-Substituted Cu4(OH)6Cl2, Phys. Status Solidi B 0, 1800663 (2019).
- [34] P. Puphal, M. Bolte, D. Sheptyakov, A. Pustogow, K. Kliemt, M. Dressel, M. Baenitz, and C. Krellner, Strong magnetic frustration in Y₃Cu₉(OH)₁₉Cl₈: a distorted kagome antiferromagnet, J. Mater. Chem. C 5, 2629 (2017).
- [35] W. Sun, Y.-X. Huang, S. Nokhrin, Y. Pan, J.-X. Mi, P. Mendels, A. S. Wills, J. X. Mi, A. Amato, J. van Tol, A. Ozarowski, A. S. Wills, P. Mendels, and A. S. Wills, Perfect Kagomé lattices in YCu₃ (OH)₆Cl₃: a new candidate for the quantum spin liquid state, J. Mater. Chem. C 4, 8772 (2016).
- [36] C. W. Hicks, M. E. Barber, S. D. Edkins, D. O. Brodsky, and A. P. Mackenzie, Piezoelectric-based apparatus for strain tuning, Rev. Sci. Instrum. 85, 65003 (2014).
- [37] M. E. Barber, A. Steppke, A. P. Mackenzie, and C. W. Hicks, Piezoelectric-based uniaxial pressure cell with integrated force and displacement sensors, Rev. Sci. Instrum. 90, 23904 (2019).
- [38] M. Hering, F. Ferrari, A. Razpopov, I. I. Mazin, R. Valentí, H. O. Jeschke, and J. Reuther, Phase diagram of a distorted kagome antiferromagnet and application to Y-kapellasite, npi Comput. Mater. 8, 10 (2022).
- [39] A. Pustogow, Y. Li, I. Voloshenko, P. Puphal, C. Krellner, I. I. Mazin, M. Dressel, and R. Valentí, Nature of optical excitations in the frustrated kagome compound Herbertsmithite, Phys. Rev. B 96, 241114(R) (2017).
- [40] Q. Barthélemy, P. Puphal, K. M. Zoch, C. Krellner, H. Luetkens, C. Baines, D. Sheptyakov, E. Kermarrec, P. Mendels, and F. Bert, Local study of the insulating quantum kagome antiferromagnets $YCu_3(OH)_6O_xCl_{3-x}(x=0,1/3)$, Phys. Rev. Mater. 3, 074401 (2019).
- [41] T. Biesner, S. Roh, A. Razpopov, J. Willwater, S. Süllow, Y. Li, K. M. Zoch, M. Medarde, J. Nuss, D. Gorbunov, Y. Skourski, A. Pustogow, S. E. Brown, C. Krellner, R. Valentí, P. Puphal, and M. Dressel, Multi-Center Magnon Excitations Open the Entire Brillouin Zone to Terahertz Magnetometry of Quantum Magnets, Adv. Quantum Technol. n/a, 2200023 (2022).
- [42] A. Zorko, M. Pregelj, M. Gomilšek, M. Klanjšek, O. Zaharko, W. Sun, and J.-X. Mi, Negative-vector-chirality 120° spin structure in the defect- and distortion-free quantum kagome antiferromagnet YCu₃(OH)₆Cl₃, Phys. Rev. B 100, 144420 (2019).
- [43] A. Zorko, M. Pregelj, M. Klanjšek, M. Gomilšek, Z. Jagličić, J. S. Lord, J. A. T. Verezhak, T. Shang, W. Sun, and J.-X. Mi, Coexistence of magnetic order and persistent spin dynamics in a quantum kagome antiferromagnet with no intersite mixing, Phys. Rev. B 99, 214441 (2019).

- [44] H. Ishikawa, M. Yoshida, K. Nawa, M. Jeong, S. Krämer, M. Horvatić, C. Berthier, M. Takigawa, M. Akaki, A. Miyake, M. Tokunaga, K. Kindo, J. Yamaura, Y. Okamoto, and Z. Hiroi, One-Third Magnetization Plateau with a Preceding Novel Phase in Volborthite, Phys. Rev. Lett. 114, 227202 (2015).
- [45] D. Boldrin and A. S. Wills, SrCu3V2O8(OH)2 dynamic Jahn–Teller distortions and orbital frustration in a new $S = \frac{1}{2}$ kagome antiferromagnet, J. Mater. Chem. C **3**, 4308 (2015).
- [46] D. Boldrin, K. Knight, and A. S. Wills, Orbital frustration in the S = 1/2 kagome magnet vesignieite, BaCu3V2O8(OD)2, arXiv:1610.01436 (2016).
- [47] S. Spachmann, P. Berdonosov, M. Markina, A. Vasiliev, and R. Klingeler, Linear magnetoelastic coupling and magnetic phase diagrams of the buckled-kagomé antiferromagnet Cu₃Bi(SeO₃)₂O₂C, Sci. Rep. 12, 7383 (2022).
- [48] K. Matan, T. Ono, Y. Fukumoto, T. J. Sato, J. Yamaura, M. Yano, K. Morita, and H. Tanaka, Pinwheel valencebond solid and triplet excitations in the two-dimensional deformed kagome lattice, Nat. Phys. 6, 865 (2010).
- [49] R. W. Smaha, W. He, J. M. Jiang, J. Wen, Y.-F. Jiang, J. P. Sheckelton, C. J. Titus, S. G. Wang, Y.-S. Chen, S. J. Teat, A. A. Aczel, Y. Zhao, G. Xu, J. W. Lynn, H.-C. Jiang, and Y. S. Lee, Materializing rival ground states in the barlowite family of kagome magnets: quantum spin liquid, spin ordered, and valence bond crystal states, npj Quantum Mater. 5, 23 (2020).
- [50] Strictly speaking, the addition/subtraction of local fields depends on the angle to the external field, which acquires various values between $[0^{\circ},180^{\circ}]$. Also, there are several inequivalent ¹H positions in the crystal structure of Y-kapellasite. Nevertheless, we expect distributions peaked at specific field values that are symmetric around B_0 . Dedicated calculations based on the $\overrightarrow{Q}=(1/3\times 1/3)$ model [38] are desired in future work.
- [51] T. Imai, É. A. Nytko, B. M. Bartlett, M. P. Shores, and D. G. Nocera, 63 Cu, 35 Cl, and 1 H NMR in the $S=\frac{1}{2}$ Kagome Lattice $\text{ZnCu}_{3}(\text{OH})_{6}\text{Cl}_{2}$, Phys. Rev. Lett. **100**, 77203 (2008).
- [52] H. Masuda, T. Okubo, and H. Kawamura, Finite-Temperature Transition of the Antiferromagnetic Heisenberg Model on a Distorted Kagome Lattice, Phys. Rev. Lett. 109, 57201 (2012).
- [53] A notable exception is Sr₂RuO₄ where the length changes upon uniaxial strain do not involve a change of bond angles [61, 63].
- [54] N. J. Laurita, A. Ron, J. W. Han, A. Scheie, J. P. Sheckelton, R. W. Smaha, W. He, J. J. Wen, J. S. Lee, Y. S. Lee, M. R. Norman, and D. Hsieh, Evidence for a Parity Broken Monoclinic Ground State in the S=1/2 Kagomé Antiferromagnet Herbertsmithite (2019), arXiv:1910.13606

- [cond-mat.str-el].
- [55] M. R. Norman, N. J. Laurita, and D. Hsieh, Valence bond phases of herbertsmithite and related copper kagome materials, Phys. Rev. Research 2, 13055 (2020).
- [56] Y. Li, A. Pustogow, M. Bories, P. Puphal, C. Krellner, M. Dressel, and R. Valentí, Lattice dynamics in the spin-½ frustrated kagome compound herbertsmithite, Phys. Rev. B 101, 161115(R) (2020).
- [57] D. P. Kozlenko, A. F. Kusmartseva, E. V. Lukin, D. A. Keen, W. G. Marshall, M. A. de Vries, and K. V. Kamenev, From Quantum Disorder to Magnetic Order in an s = 1/2 Kagome Lattice: A Structural and Magnetic Study of Herbertsmithite at High Pressure, Phys. Rev. Lett. 108, 187207 (2012).
- [58] M. Jeong, F. Bert, P. Mendels, F. Duc, J. C. Trombe, M. A. de Vries, and A. Harrison, Field-Induced Freezing of a Quantum Spin Liquid on the Kagome Lattice, Phys. Rev. Lett. 107, 237201 (2011).
- [59] M. S. Grbić, S. Krämer, C. Berthier, F. Trousselet, O. Cépas, H. Tanaka, and M. Horvatić, Microscopic Properties of the Pinwheel Kagome Compound Rb₂Cu₃SnF₁₂, Phys. Rev. Lett. 110, 247203 (2013).
- [60] D. Chatterjee, P. Puphal, E. Kermarrec, Q. Barthelemy, S. Petit, J. Willwater, S. Süllow, C. Baines, E. Ressouches, J. Ollivier, K. Zoch, C. Krellner, M. Parzer, A. Riss, F. Garmroudi, A. Pustogow, P. Mendels, and F. Bert, From quantum spin liquid to long range order in the distorted kagome system Y-Kapellasite, Y₃Cu₉(OH)₁₈OCl₈, in preparation (2022).
- [61] Y. Luo, A. Pustogow, P. Guzman, A. P. Dioguardi, S. M. Thomas, F. Ronning, N. Kikugawa, D. A. Sokolov, F. Jerzembeck, A. P. Mackenzie, C. W. Hicks, E. D. Bauer, I. I. Mazin, and S. E. Brown, Normal State ¹⁷O NMR Studies of Sr₂RuO₄ under Uniaxial Stress, Phys. Rev. X 9, 21044 (2019).
- [62] A. Chronister, M. Zingl, A. Pustogow, Y. Luo, D. Sokolov, N. Kikugawa, C. Hicks, F. Jerzembeck, J. Mravlje, E. Bauer, A. Mackenzie, A. Georges, and S. Brown, Tuning the Fermi Liquid Crossover in Sr₂RuO₄ with Uniaxial Stress (2021), arXiv:2111.05570 [condmat.str-el].
- [63] A. Steppke, L. Zhao, M. E. Barber, T. Scaffidi, F. Jerzembeck, H. Rosner, A. S. Gibbs, Y. Maeno, S. H. Simon, A. P. Mackenzie, and C. W. Hicks, Strong peak in T_c of Sr₂RuO₄ under uniaxial pressure, Science 355, eaaf9398 (2017).
- [64] M. E. Barber, F. Lechermann, S. V. Streltsov, S. L. Skornyakov, S. Ghosh, B. J. Ramshaw, N. Kikugawa, D. A. Sokolov, A. P. Mackenzie, C. W. Hicks, and I. I. Mazin, Role of correlations in determining the Van Hove strain in Sr₂RuO₄, Phys. Rev. B 100, 245139 (2019)

•